ORIGINAL RESEARCH

Cytotoxic effects of ZnO nanoparticles on mouse testicular cells

Zhe Han[1],*
Qi Yan[1],*
Wei Ge[2]
Zhi-Guo Liu[1]
Sangiliyandi Gurunathan[3]
Massimo De Felici[4]
Wei Shen[2]
Xi-Feng Zhang[1]

[1]College of Biological and Pharmaceutical Engineering, Wuhan Polytechnic University, Wuhan, People's Republic of China; [2]Key Laboratory of Animal Reproduction and Germplasm Enhancement in Universities of Shandong, College of Animal Science and Technology, Qingdao Agricultural University, Qingdao, People's Republic of China; [3]Department of Stem Cell and Regenerative Biology, Konkuk University, Seoul, Republic of Korea; [4]Department of Biomedicine and Prevention, University of Rome "Tor Vergata", Rome, Italy

*These authors contributed equally to this work

Correspondence: Xi-Feng Zhang
College of Biological and Pharmaceutical Engineering, Wuhan Polytechnic University, Wuhan 430023, People's Republic of China
Email zhangxf9465@163.com

Background: Nanoscience and nanotechnology are developing rapidly, and the applications of nanoparticles (NPs) have been found in several fields. At present, NPs are widely used in traditional consumer and industrial products, however, the properties and safety of NPs are still unclear and there are concerns about their potential environmental and health effects. The aim of the present study was to investigate the potential toxicity of ZnO NPs on testicular cells using both in vitro and in vivo systems in a mouse experimental model.

Methods: ZnO NPs with a crystalline size of 70 nm were characterized with various analytical techniques, including ultraviolet-visible spectroscopy, Fourier transform infrared spectroscopy, X-ray diffraction, transmission electron microscopy, and atomic force microscopy. The cytotoxicity of the ZnO NPs was examined in vitro on Leydig cell and Sertoli cell lines, and in vivo on the testes of CD1 mice injected with single doses of ZnO NPs.

Results: ZnO NPs were internalized by Leydig cells and Sertoli cells, and this resulted in cytotoxicity in a time- and dose-dependent manner through the induction of apoptosis. Apoptosis likely occurred as a consequence of DNA damage (detected as γ-H2AX and RAD51 foci) caused by increase in reactive oxygen species associated with loss of mitochondrial membrane potential. In addition, injection of ZnO NPs in male mice caused structural alterations in the seminiferous epithelium and sperm abnormalities.

Conclusion: These results demonstrate that ZnO NPs have the potential to induce apoptosis in testicular cells likely through DNA damage caused by reactive oxygen species, with possible adverse consequences for spermatogenesis and therefore, male fertility. This suggests that evaluating the potential impacts of engineered NPs is essential prior to their mass production, to address both the environmental and human health concerns and also to develop sustainable and safer nanomaterials.

Keywords: ZnO nanoparticle, Sertoli cells, Leydig cells, mice

Introduction

Nanotechnology, the manipulation of matter at the atomic, molecular, and supramolecular scales, is a rapidly developing area, offering new prospects in many industrial sectors. In nanotechnology, nanoparticles (NPs) are defined as particles of 1–100 nm in size that behave as whole units with respect to their transport and properties. NPs have a greater surface area per weight than larger particles, making them more reactive than larger particles to some other molecules. NPs are used in many fields, including medicine, manufacturing and materials, energy, electronics, and environmental applications.[1–5] Metal oxide nanostructures are one of the most abundantly produced types of engineered nanomaterials, and are used widely in both advanced research and emerging technologies. ZnO NPs are well known and widely used as metal oxides in many diverse products, and also as catalysts in electronics,

clothing, paints, coatings, and cosmetic products.[6–8] The biological applications of ZnO NPs have received particular attention, including their use as biosensors and in medical devices. This broad spectrum of applications leads to increased human and environmental exposure to these NPs and therefore, an increase in potential risk due to their short- and long-term toxicity. The increased use of ZnO NPs in consumer products on the market and the devastating long-term damage they potentially cause to humans have prompted increased assessment of their adverse effects in vitro and in vivo.[9,10]

Several studies have reported the cytotoxic and genotoxic potential of ZnO NPs using in vitro assays in immune cells, lung epithelial, and cancer cells.[11–14] Johnson et al showed that the exposure of immune cells to ZnO NPs resulted in increased levels of the autophagosome protein LC3A and, consequently, autophagic death, which were inhibited by blocking autophagy and reactive oxygen species (ROS) production.[11] Sharma et al reported that ZnO NPs induced DNA damage in human epidermal cells, even at low concentrations, which may have been mediated by lipid peroxidation and oxidative stress.[12] These authors also demonstrated that ZnO NPs were internalized by human epidermal keratinocytes and elicited cytotoxic and genotoxic responses.[13] Other studies showed that ZnO NPs were cytotoxic for human lung epithelial cells and induced cell-cycle arrest, cell apoptosis, ROS production, mitochondrial dysfunction, and perturbation of glucose metabolism in such cells.[14,15] Increasing evidence has shown that the cytotoxicity of ZnO NPs is mediated by the generation of oxidative stress, involving the induction of lipid peroxidation and ROS-dependent DNA damage. Ahamed et al reported that ZnO NPs induced apoptosis in A549 cells, a type II pulmonary epithelial cell line, through ROS and oxidative stress by the TP53, survivin, Bax/Bcl-2, and caspase pathways.[16] Ng et al also found that ZnO NP treatment caused a reduction in BJ cell (skin fibroblast) numbers, which required TP53 as the molecular master switch, moving the cells toward programmed cell death.[17]

Leydig cells (LCs) and Sertoli cells (SCs), the two major somatic cell types in the mammalian testes, have different morphologies and functions, and both are essential for gonad development and spermatogenesis. LCs are known to play a crucial role in the synthesis of the steroid testosterone and in the regulation of spermatogenesis, sperm maturation, and sexual function.[18–20] SCs, located within the seminiferous tubules of the testis, provide nutrition and morphogenetic support for the germ cells during spermatogenesis, offer structural support for the developing germ cells, create a cellular barrier between the testes and the immune system, synthesize essential factors for developing germ cells, and are involved in the formation of the blood–testis barrier.[21,22] Consequently, they play critical roles in the maintenance and control of spermatogonial self-renewal and survival. Therefore, LCs and SCs are potential targets in the reproductive dysfunction induced by environmental toxicants in male mice. Any agent that impairs the viability and functions of these two cell types will have profound effects on spermatogenesis.[23–25]

Concerning the effect of ZnO NP on male reproduction, it has been reported that these NPs can act as a testicular toxicant.[26–28] Ji et al have reported that LCs exposed to 10/20 μM of cadmium (Cd) had reduced levels of steroid hormone due to inhibition of activation of cyclic adenosine monophosphate/protein kinase A, protein kinase C signaling pathway, and the steroidogenic enzymes StAR, CYP11A1, and 3β-HSD.[26] Also, Talebi et al reported that epithelial vacuolization, sloughing of germ cells, and detachment of mice were significantly increased after treatment with ZnO NPs, and also, ZnO NPs caused a significant decrease in seminiferous tubule diameter, seminiferous epithelium height, and maturation arrest.[28] But the cytotoxic mechanism of ZnO NPs in LCs and SCs are still poorly known. Due to the lack of information regarding the reproductive toxicity of ZnO NPs, the present study was designed to investigate the possible cytotoxic effects of ZnO NPs on testicular LCs and SCs.

Materials and methods
Characterization of ZnO NPs

ZnO NPs (about 70 nm) were obtained from Beijing DK nanotechnology Co. Ltd (Beijing, People's Republic of China). The size, shape, and dispersion of ZnO NPs were evaluated by transmission electron microscopy (TEM) (H-7500; Hitachi Ltd., Tokyo, Japan) and dynamic light scattering (DLS) (ZetaPals; Brookhaven Instruments Corporation, Long Island, NY, USA). X-ray diffraction (XRD) data were collected on a D8 Advance X-ray Powder Diffractometer (Bruker Optik GmbH, Ettlingen, Germany). The specimens were examined using an S-3000N scanning electron microscope (SEM) system (Hitachi Ltd.) operated at 15 kV. The surface chemical bonding and composition of NPs were characterized using a Fourier transform infrared spectroscopy (FTIR) instrument (PerkinElmer Spectroscopy GX, Branford, CT, USA). Atomic force microscopy (AFM) was used for evaluating the surface morphology and properties of the ZnO NPs.

Cell culture and exposure of cells to ZnO NPs

LCs and SCs were cultured in HyClone™ Dulbecco's Modified Eagles Medium (DMEM) (GE Healthcare Bio-Sciences, Marlborough, MA, USA) supplemented with fetal bovine serum (10%) and antibiotics (penicillin 100 U/mL and streptomycin 100 μg/mL) at 37°C in 5% CO_2 atmosphere. Cells were seeded at a density of 1×10^4 cells per well and cultured for 24 hours before washing with phosphate-buffered saline (PBS; pH 7.4) and incubated in a fresh medium containing different concentrations of ZnO NPs as indicated in the "Results" section. ZnO NPs were sonicated before use in cell culture.

Cytotoxicity assays

Intracellular 3-(4,5-dimethylthiazol-2-yl)-2,5-diphenyltetrazolium bromide (MTT) levels were evaluated as described by Zhang et al[29] and lactate dehydrogenase (LDH) leakage assay was performed according to the manufacturer's instructions (LDH Assay kit; Abcam, Cambridge, MA, USA); they were used as NP cytotoxicity parameters. Cell-free control experiments were performed to determine the reactivity of the ZnO NPs with the MTT reagent. Typically, 100 μL of ZnO NP suspensions with different concentrations was added to a 96-well plate and 10 μL of MTT reagent solution was added to each well; the mixture was incubated at 37°C under 5% CO_2 for 1 hour. After incubation, the ZnO NPs were centrifuged and 100 μL of the supernatant was transferred to another 96-well plate. The optical density was measured at 450 nm.

Evaluation of ROS levels

Intracellular ROS levels were measured using the detection kit n. S0033 purchased from Beyotime (Jiangsu, People's Republic of China). Briefly, cells were seeded in six-well plates for 24 hours and incubated with fresh medium containing 10 μM dichloro-dihydro-fluorescein diacetate at 37°C in the dark for 20 minutes. Subsequently, the cells were treated with different concentrations of ZnO NPs for 6 hours. At the end of incubation, the cells were washed with PBS and the dichlorofluorescein fluorescence intensity measured under a fluorescence microscope using image analysis software. Images were captured with an electronic camera (Olympus Corporation, Tokyo, Japan; 100× magnification).

Cellular uptake of ZnO

Ultrathin sections of cells were analyzed using TEM to determine the distribution of NPs. Briefly, the cells (treated with 15 μg/mL ZnO NPs, 12 hours) were fixed in 2.5% glutaraldehyde for 2 hours, and the samples dehydrated in an ethanol series and embedded in epoxy resin following standard procedures.

TUNEL and JC-1 assays

TUNEL analysis was performed to quantify cell apoptosis using the In Situ Cell Death Detection Kit, Fluorescein, purchased from Roche Diagnostics (Indianapolis, IN, USA) according to the manufacturer's instructions. Cells were cultured with 15 μg/mL ZnO NPs for 0, 3, 6, and 12 hours, and then washed in PBS, fixed in 4% paraformaldehyde for 15 minutes, and incubated in a TUNEL reaction mixture for 2 hours at 37°C.

JC-1 assay was performed according to the manufacturer's instructions (JC-1 Mitochondrial Membrane Potential Assay Kit; Abnova, Taipei City, Taiwan). Cells were cultured with 15 μg/mL ZnO NPs for 0, 3, 6, and 12 hours under the conditions described above. They were then transferred onto a coverslip housed in a four-well plate and incubated in DMEM containing 10 μM JC-1 at 37°C for 15 minutes before they were washed with PBS and rapidly mounted for observation. In all procedures, cells were mounted with Vectashield fluorescence medium and visualized under a fluorescent microscope.

Number of cells with abnormal nucleus

Cells were treated with ZnO NPs at the concentration of 0, 5, 10, 15, and 20 μg/mL for 12 and 24 hours. After washing with PBS, the cells were counterstained with 4′,6-diamidino-2-phenylindole (DAPI) and visualized with a confocal microscope (Leica TCS SP5 II; Leica Microsystems, Wetzlar, Germany). All cell samples were scored for the presence of DNA leakage, and more than one leaked DNA or captured DNA by autophagosomes per cell reflects ZnO NPs-induced DNA damage.

In situ detection of DNA breaks

Cells incubated with ZnO NPs for 12 hours were fixed in 4% paraformaldehyde and blocked with 1% bovine serum albumin for 30 minutes. They were then incubated with primary antibodies against γ-H2AX (ab26350; Abcam) or Rad51 (ab88572; Abcam) at 4°C overnight. After washing with PBS, the cells were labeled with Cy3-labeled goat antirabbit immunoglobulin G at a dilution of 1:50 (A0516, Beyotime) at 4°C for 1.5 hours. Finally, the samples were counterstained with DAPI and visualized under a confocal microscope (Carl Zeiss LSM 780; Instrument Development Center, NCKU, Taiwan).

Western blot analyses

For Western blot analysis, the harvested cell pellets were incubated in radioimmunoprecipitation assay lysis buffer in the presence of a protease inhibitor. Protein concentrations were measured using BCA Protein Assay Reagent (Pierce, Rockford, IL, USA). The cell lysates were then analyzed for protein content using sodium dodecyl sulfate-polyacrylamide gel electrophoresis. The membrane was probed with antibodies to determine the levels of protein expression. The following primary antibodies were used: anti-γ-H2AX (ab26350; Abcam), anti-RAD51 (ab88572; Abcam), and anti-β-actin antibody (ab8227; Abcam).

Exposure of mice to ZnO NPs

The study and animal care were approved by the Ethical Committee of Wuhan Polytechnic University. The mice used in this study were provided by the Institute of Poultry Science of the Chinese Academy of Agriculture Sciences. Procedures involving the care and use of animals conformed to the US National Institutes of Health guidelines (NIH Pub No 85-23, revised 1996). Twenty-one day old (postnatal day [PND]21) CD-1 mice were purchased for this study from Vital River, (Beijing, People's Republic of China) and housed in temperature-controlled (21°C–22°C) and light-controlled (12 h light, 12 h dark cycle) conditions. The mice were divided into three groups (more than six animals per group) as follows: group 1, control; group 2, 1.0 mg/kg ZnO NP-treated group; and group 3, 5.0 mg/kg ZnO NP-treated group. The control group received water, whereas the treated groups received intravenous tail injection of ZnO NPs. Testes were collected at PND28 and PND42 and fixed in 4% paraformaldehyde for standard histological procedures. Each testis was sliced into 5 μm sections, and representative sections were selected every ten sections for evaluation. A total of six testes from six mice were obtained from each group. Slices were imaged under a light microscope (Olympus BX51, Olympus Corporation).

Sperm analysis

At PND49, the epididymides were dissected from control and treated mice. Sperm were isolated from the caudae by dispersion in Medium 199 (supplemented with 0.5% bovine serum albumin) at 37°C for 10 minutes. The sperm samples were then smeared onto a slide, fixed in 10% neutral buffered formalin, and stained with 1% eosin solution. The morphology of >500 sperm from each sample was examined under a microscope.

Statistical analysis

Data are presented as the mean ± standard deviation (SD) of three independent experiments, each done in triplicate. Differences between the means were evaluated by the Student's t-test or one-way analysis of variance followed by Tukey's test for multiple comparisons using the GraphPad Prism software (GraphPad Software, Inc., La Jolla, CA, USA). The differences were considered significant at $P < 0.05$.

Results and discussion
Analysis of ZnO NPs with TEM, SEM, and DLS

Characterization of NPs is an essential process before evaluation of toxicity potential of ZnO NPs. TEM is one of the most effective techniques to analyze the size and morphology of NPs.[30] TEM micrographs of the ZnO NPs revealed distinct, uniformly spherical, well-separated particles (Figure 1A). The average particle size was estimated from measurements of >100 particles in TEM images. The mean size ± SD of the particles was calculated in random fields of view and from images that showed the general morphology of the NPs (Figure 1B). The SEM images (Figure 1C) showed that the ZnO NPs were polydispersed in nature and agglomerated into quasispherical to hexagonal structures. These characteristics are consistent with those of ZnO NPs prepared by solvothermal processes and indicate that the produced ZnO NPs possess a narrow size distribution and quasispherical to hexagonal shapes which are suitable for further toxicity studies.[31] Particle size distribution was performed by DLS, which showed the average size as between 20 and 110 nm (Figure 1D).

XRD analysis of ZnO NPs

XRD analysis confirmed the crystalline nature of the particles. A representative XRD pattern is shown in Figure 2A. The profile shows seven peaks in the whole spectrum of 2θ values at 31.7°, 34.4°, 36.2°, 47.5°, 56.6°, 62.8°, and 68.0°.[32] These strong narrow diffraction peaks are indicative of the crystalline structure of the NPs. The sizes of ZnO NPs predicted from XRD data are consistent with Joint Committee on Powder Diffraction Standards file no 00-036-1451. The positions of diffraction peaks for ZnO NPs are identical to those of the standard zincite structure (Joint Committee on Powder Diffraction Standards file no 00-036-1451). The peaks at 2θ values of 31.7°, 34.4°, and 36.2° can be assigned to the (100), (002), and (101) crystal planes of the hexagonal phase of ZnO. Based on the XRD data of the (101) reflection band, suggesting that the ZnO NPs had crystalline nature. Furthermore, the profile validated the purity of NPs since it contained only characteristic XRD peaks.
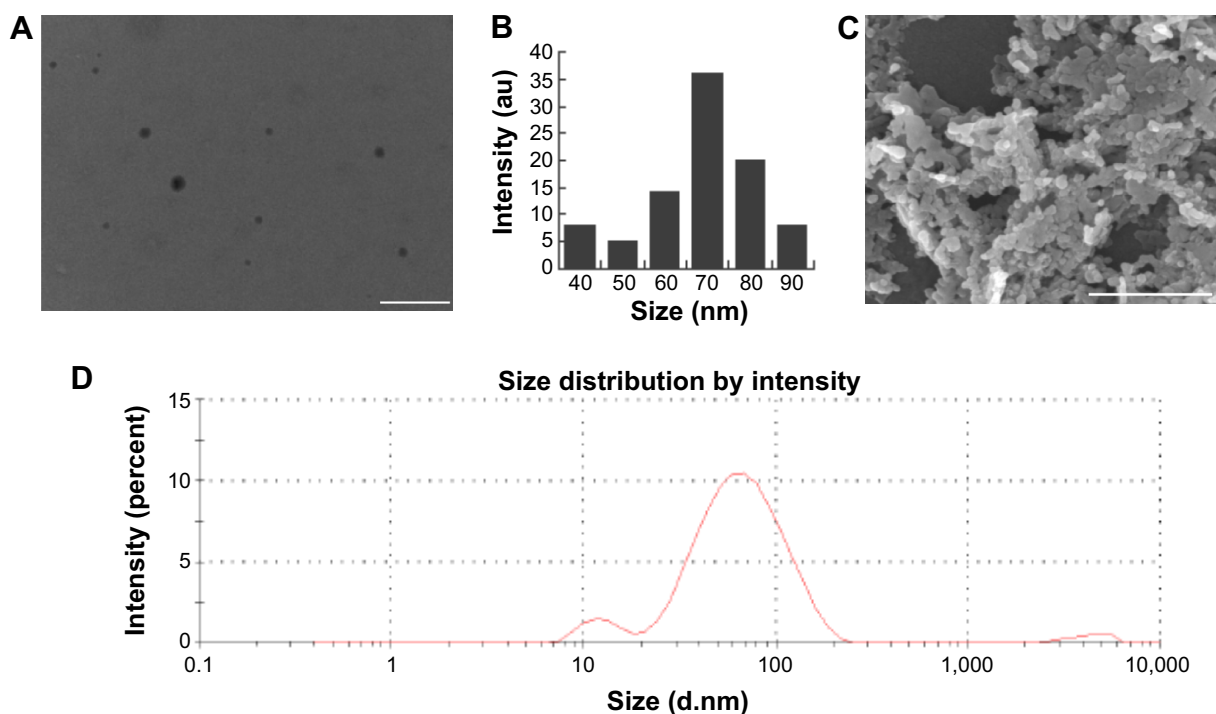
Figure I Characterization of ZnO NPs by TEM, SEM, and DLS.
Notes: (**A**) A representative TEM and (**B**) size distribution of ZnO NPs scored on several fields of TEM images. (**C**) SEM 8B9 images of ZnO NPs. (**D**) Measurement of size distribution of ZnO NPs by DLS. Scale bars =150 μm.
Abbreviations: au, absorbance units; DLS, dynamic light scattering; NPs, nanoparticles; SEM, scanning electron microscopy; TEM, transmission electron microscopy.

FTIR spectra of ZnO NPs

Infrared studies were performed to confirm the purity and the metal nature of NPs. Figure 3 shows the FTIR spectra of ZnO NPs. The FTIR measurements of the ZnO NPs showed peaks at 3,440 cm^{-1} (phosphorous compounds, secondary sulfonamide), 2,922 cm^{-1} (monosubstituted alkynes, β-lactones, amine salts), 1,627 cm^{-1} (medium charge vinyl, *cis*-tri substituted), 1,396 cm^{-1} (amide II), and 1,047 cm^{-1} (monosubstituted alkyne) (Figure 2B).[33] The peaks observed at 3,440 and 1,047 cm^{-1} indicate O–H stretching and deformation, respectively, assigned to the water adsorption on the metal surface. The peaks at 1,627 and 439 cm^{-1} correspond to Zn–O stretching and deformation vibration, respectively. These data are in line with those of ZnO NPs prepared by the microemulsion route.[33]

Characterization of ZnO NPs with AFM

AFM is an instrument for the morphological characterization of ZnO NPs and can be used to image and evaluate their surface morphology and property.[34] Figure 3A is a typical AFM image of ZnO NPs' dispersion in water after their deposition on a freshly cleaned glass surface. The average width of the ZnO NPs measured from the AFM image was A–B 58.27 nm and C–D 67.61 nm (Figure 3B). The data derived from the AFM support those obtained from the TEM and XRD analyses. Eita

et al observed that ZnO NPs stabilized with cationic surfactant showed high surface roughness of 22.9 nm, in comparison with the average thickness of the film and the size of the ZnO NPs (99 nm), indicating that the multilayer is highly porous with random adsorption of ZnO NPs.[35]

ZnO NPs are internalized and accumulated within autophagosomes by LCs and SCs

In order to investigate the effect of ZnO NPs on testicular cells, we began to culture LCs and SCs in the presence of increasing concentrations of ZnO NPs. Cells were incubated with the particles at a concentration of 5 μg/mL for 12 and 24 hours, and were then fixed and prepared for TEM observation. As shown in Figure 4A, aggregates of ZnO NPs were found localized within the cytoplasm and, in some cases, into the nucleus. In this organelle compared with the control group (Figure 4B[a]), we observed abnormal expansion of the intermembrane space of the nuclear membrane (Figure 4B[b, c]). Moreover, particles were often observed within vesicles (Figure 4B[d]). We used fluorescence microscopy to examine the LC3 (anti-LC3B, ab51520; Abcam) expression of the ZnO NP-treated LCs and SCs. As shown in Figure S1, the treatment of cells with ZnO NPs consistently induced LC3 expression. Interestingly, studies
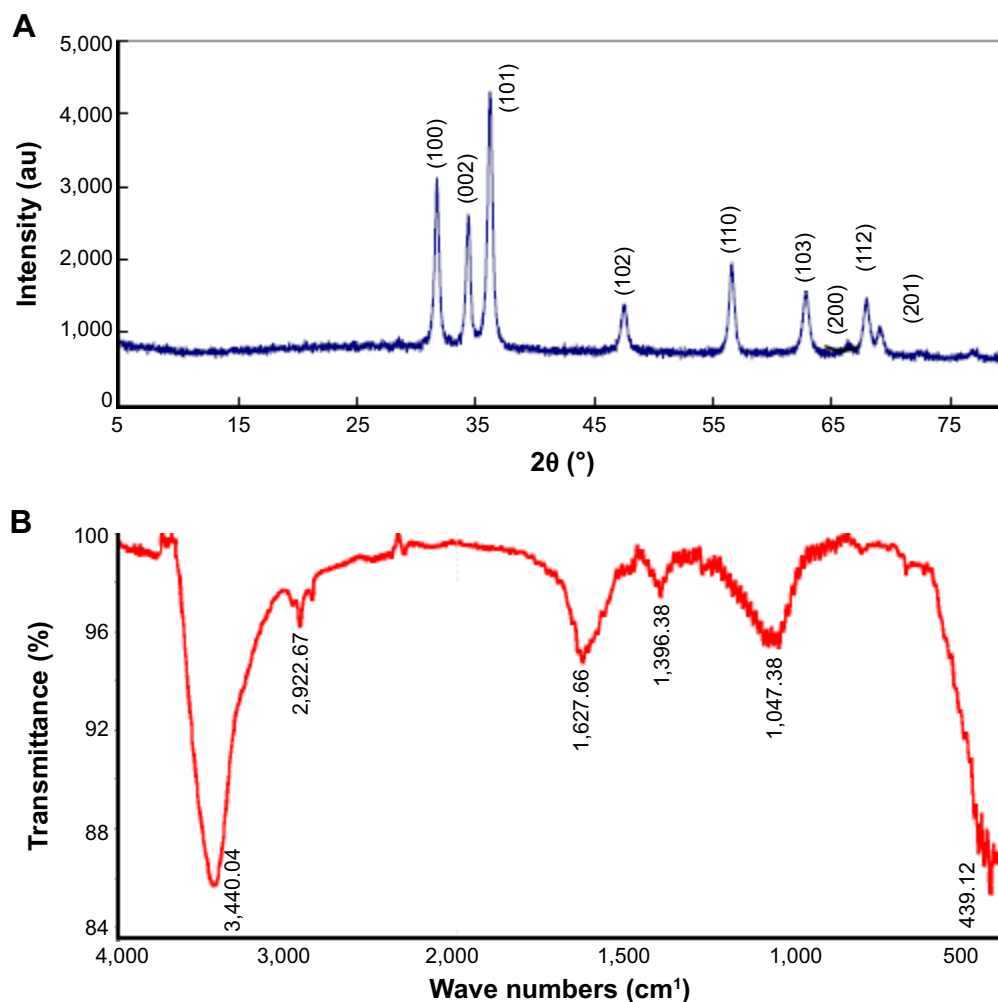
Figure 2 XRD and FITR spectra of ZnO NPs.

Notes: (**A**) XRD spectrum; note seven intense peaks across the spectrum of 2θ values ranging from 25° to 75°. The peaks at 2θ = 31.7°, 34.4°, 36.2°, 47.5°, 56.6°, 62.8°, 66.28°, 68.0°, 69.03°, and 72.48° were assigned to (100), (002), (101), (102), (110), (103), (200), (112), and (201) of ZnO NPs, indicating that the samples were polycrystalline wurtzite structure (Zincite, JCPDS 5-0664). No characteristic peaks of any impurities were detected, suggesting that high-quality ZnO NPs were synthesized. (**B**) FITR spectra show peaks at 3,440 cm^{-1} (phosphorous compounds, secondary sulfonamide), 2,922 cm^{-1} (monosubstituted alkynes, β-lactones, amine salts), 1,627 cm^{-1} (medium charge vinyl, *cis*-tri substituted), 1,396 cm^{-1} (amide II), and 1,047 cm^{-1} (monosubstituted alkyne).

Abbreviations: au, absorbance units; FITR, Fourier transform infrared spectroscopy; NPs, nanoparticles; XRD, X-ray diffraction.

performed in cultured JB6Cl41-5 (a mouse skin epidermal cell line) showed that ZnO NPs increased the number of autophagosomes and the expression of autophagic proteins such as microtubule-associated protein light chain 3-isoform II (MAP-LC3-II) and Beclin 1, through the inhibition of phosphorylation of Akt, PI3K, and mTOR.[36]

## Cytotoxicity of ZnO NPs and apoptosis induction

In order to evaluate the cytotoxicity of ZnO NPs on LCs and SCs, we assessed the mitochondrial function using MTT, conducted cellular metabolic activity assay, and determined cell membrane integrity loss (as LDH leakage into the culture medium assay),[35] which are the endpoints of cytotoxicity. Both the MTT and LDH assays indicated time- and concentration-dependent cytotoxicity of ZnO NPs on both cell lines (Figure 5A–D). While analyzing the cell viability with various concentrations of ZnO NPs, significant cytotoxicity was observed between 15 and 20 μg/mL, whereas cytotoxicity assays such as LDH showed a significant effect from 10 to 20 μg/mL. To determine the difference between control and treated samples in the LDH assay, the leakage of LDH in the control was set at onefold. As shown in Figure S2, the ZnO NP toxicity was dependent on the particle and not on the released Zn^{2+}. These results are in line with previous studies showing that silver NPs caused cytotoxicity in LCs and SCs of testes in neonatal mice.[33]

In the next series of experiments, we found that ZnO NP cytotoxicity was a likely consequence of apoptosis induced
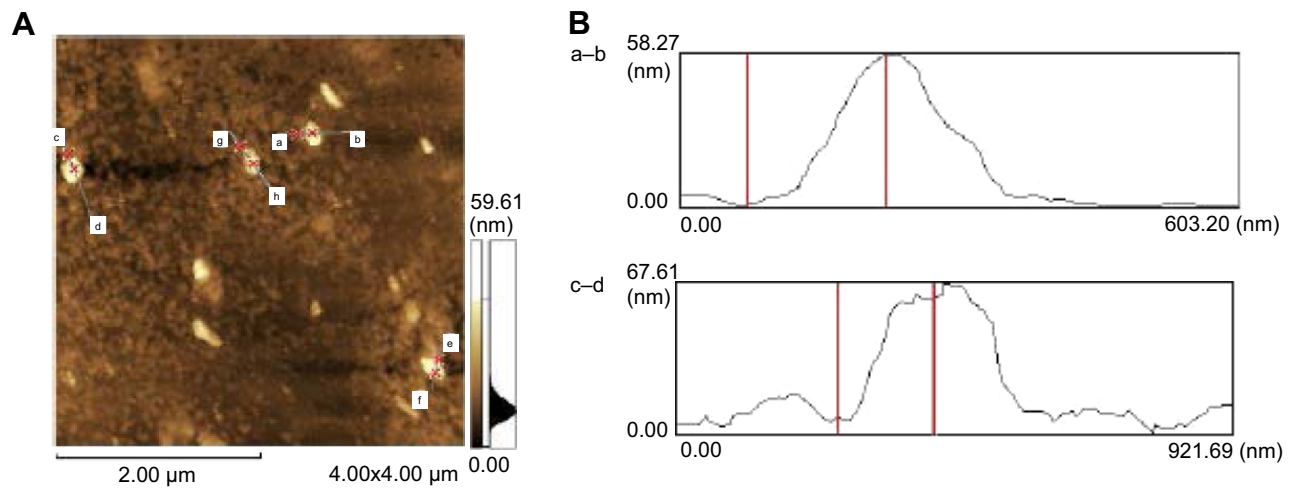
Figure 3 Scanning probe microscopy of noncontact AFM images of the ZnO NPs.
Notes: (**A**) Analysis of individual particle sizes (a–h). (**B**) a–b size is 58.27 nm and c–d size is 67.61 nm.
Abbreviations: AFM, atomic force microscopy; NPs, nanoparticles.
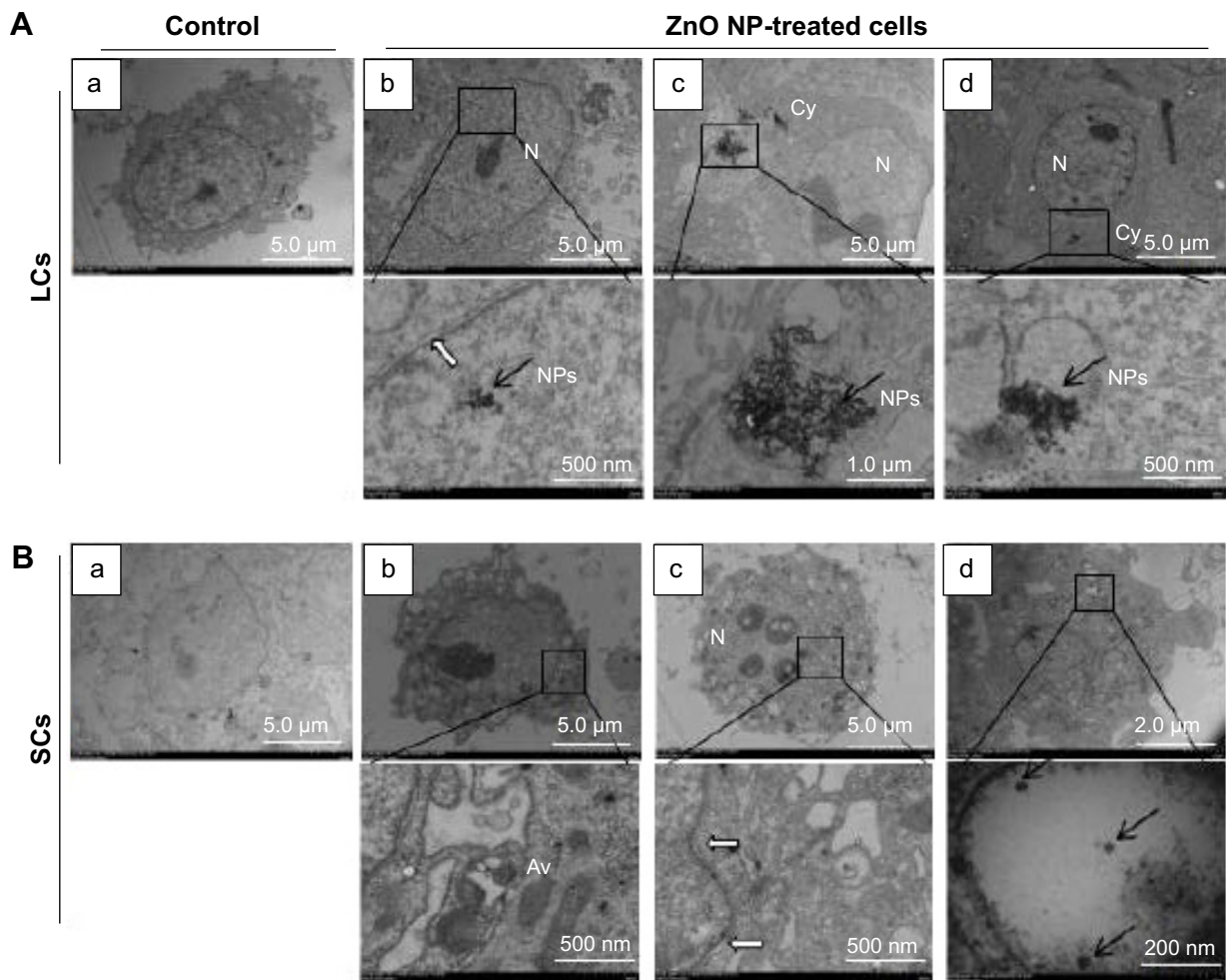
Figure 4 TEM observations of ZnO NP internalization by LCs and SCs.
Notes: (**A**) (a) Untreated LCs, (b–d) localization of ZnO NPs within the Cy and N of the LCs; bottom row = magnifications of the framed region. (**B**) (a) Untreated SCs, (b–d) localization of ZnO NPs within the SCs; bottom row = magnifications of the framed region. Black arrows indicate ZnO NPs and white arrows indicate the intramembranous space between the inner and outer membranes of the nuclear envelope.
Abbreviations: Av, autophagic vacuoles; Cy, cytoplasm; LCs, Leydig cells; N, nucleus; NPs, nanoparticles; SCs, Sertoli cells; TEM, transmission electron microscopy.
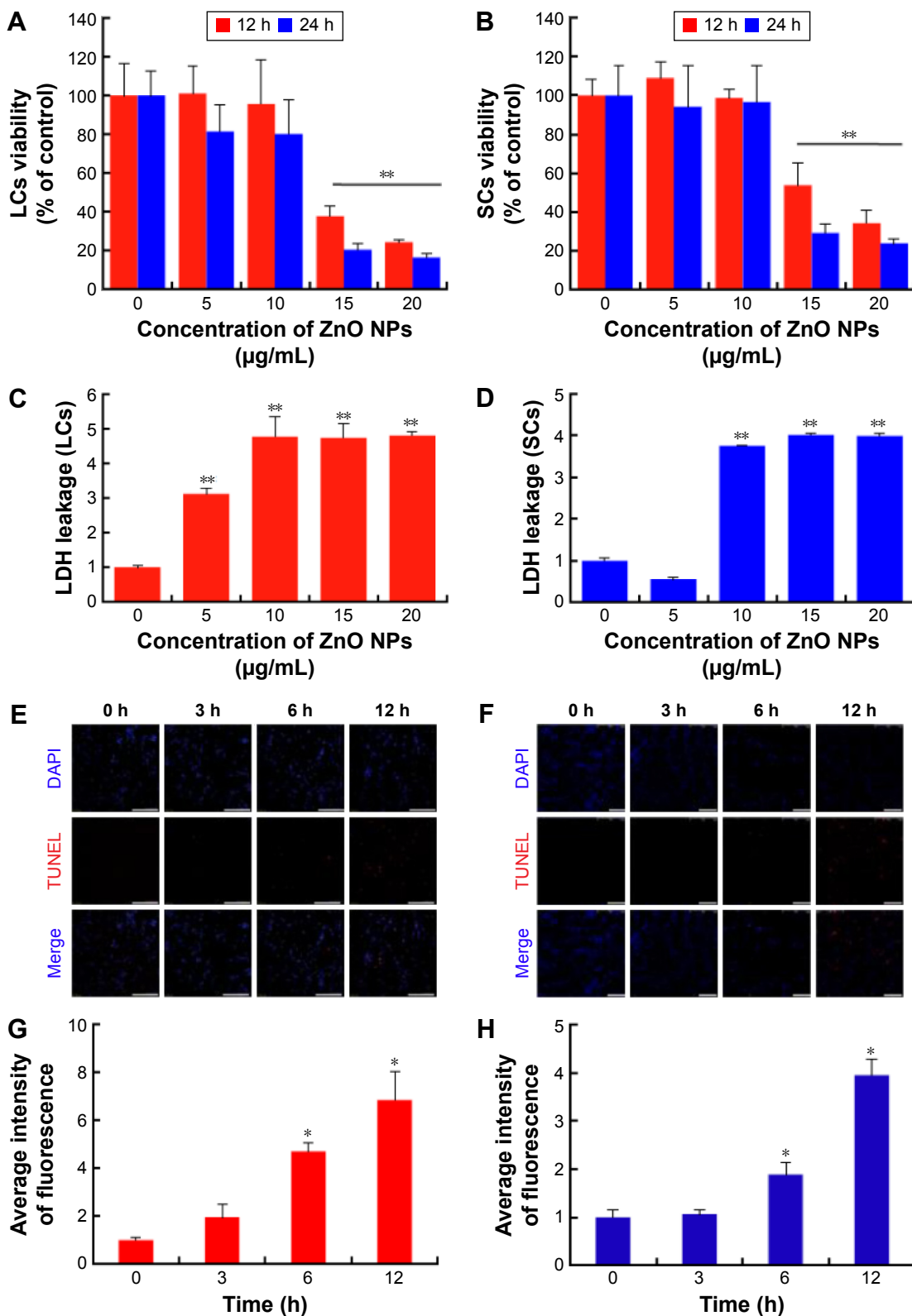
Figure 5 Viability and TUNEL histochemistry of LCs and SCs after ZnO NP treatments.

Notes: In order to verify ZnO NPs cytotoxicity, cells were treated with various concentrations of ZnO NPs for 12 and 24 h and viability determined with (**A** and **B**) MTT and (**C** and **D**) LDH assays. (**E** and **F**) Apoptosis was detected by the TUNEL histochemistry in cells treated for 0, 3, 6, and 12 h with 15 μg/mL ZnO NPs. (**A**, **C**, **E**, and **G**) are the data of LCs; (**B**, **D**, **F**, and **H**) are the data of SCs. Scale bars =150 μm. The results are expressed as the mean ± standard deviation of three separate experiments, in triplicate. *P<0.05, **P<0.01.

Abbreviations: DAPI, 4′,6-diamidino-2-phenylindole; LCs, Leydig cells; LDH, lactate dehydrogenase; MTT, 3-(4,5-dimethylthiazol-2-yl)-2,5-diphenyltetrazolium bromide; NPs, nanoparticles; SCs, Sertoli cells; TUNEL, terminal deoxynucleotidyl transferase dUTP nick end labeling; TEM, transmission electron microscopy; h, hours.

by the NPs in LCs and SCs. In fact, the number of cells staining positive for TUNEL histochemistry, commonly used to show the presence of apoptotic cells, increased as a function of the culture time and the concentration of the ZnO NPs in the medium (Figure 5E–H).

ZnO NPs induce increased ROS level and loss of mitochondrial membrane potential

We found that the decrease in cell viability and the increase in the number of TUNEL-positive LCs and SCs caused by ZnO NP exposure were associated to a marked increase in ROS level in both cell types after 6 hours of culture, monitored by the fluorescent probe (dichloro-dihydro-fluorescein

diacetate) (Figure 6A), suggesting ongoing ROS-triggered apoptosis. Consistently, the generation of ROS and consequent apoptosis induction are considered the common adverse effects of many types of synthesized NPs, including ZNO NPs.[37–44] In particular, ZnO NPs have been reported to induce oxidative stress and apoptosis in HepG2 and MCF-7 cells through upregulation of the mRNA expression levels of Bax, p53, and caspase-3 and downregulation of the antiapoptotic gene Bcl-2.[45] Moreover, ZnO NPs were found to be cytotoxic for the human liver cell line HepG2 by increasing the ROS levels and, consequently, causing a decrease in mitochondrial membrane potential and an increase in the ratio of Bax/Bcl-2.[46] Mitochondria are generally the main source of cellular ROS and a loss
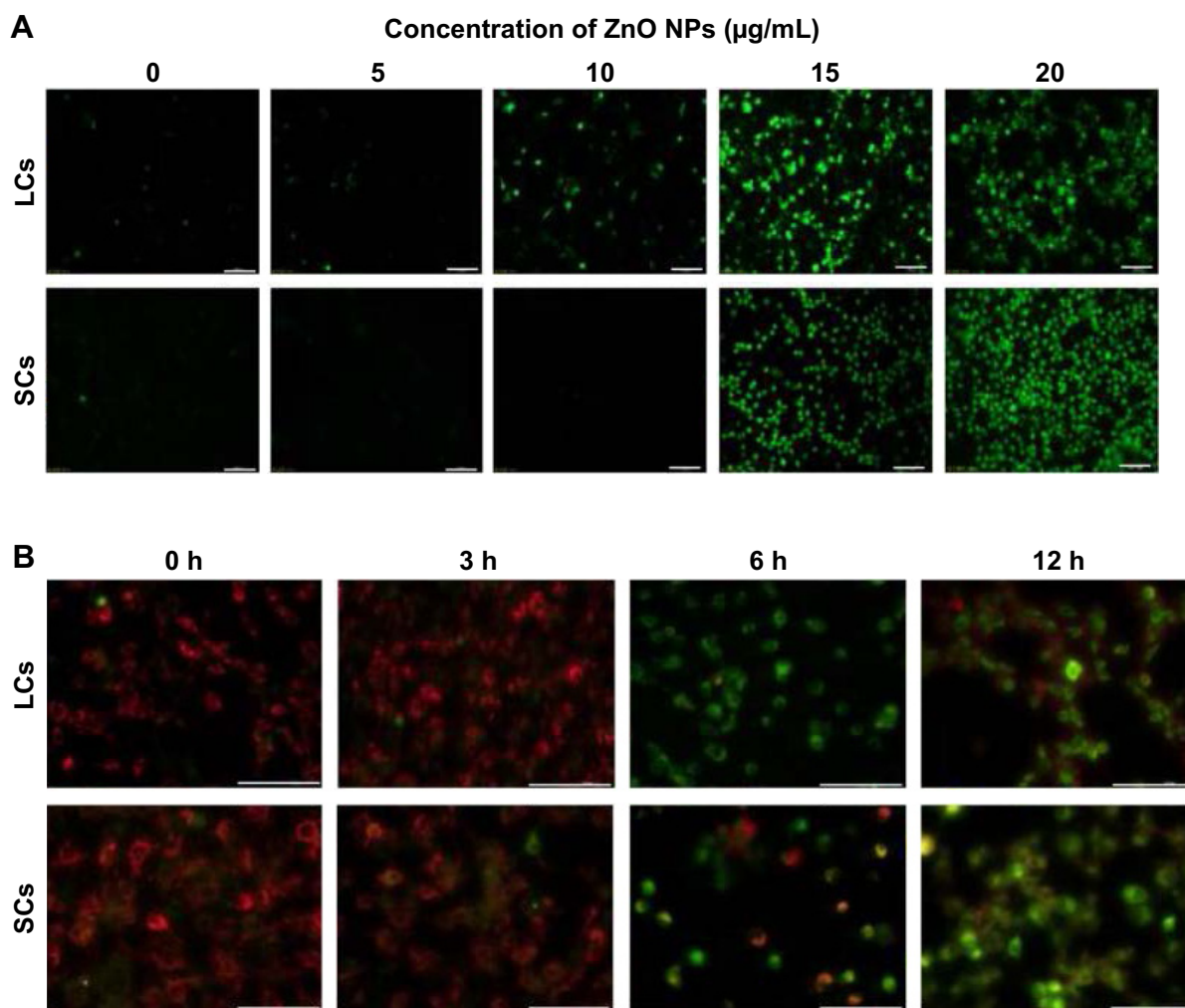
Figure 6 Evaluation of ROS level and mitochondrial membrane potential in LCs and SCs after ZnO NP treatment.
Notes: (**A**) Intracellular ROS levels were measured with fluorescence imaging using the DCFH-DA probe in cells cultured in the presence of increasing concentration of ZnO NPs for 6 hours. Scale bars =100 μm. (**B**) Mitochondrial membrane potential (ΔΨm) was evaluated using JC-1 in cells treated with 15 μg/mL ZnO NPs for 0, 3, 6, and 12 hours. Red fluorescence indicates JC-1 aggregates within the mitochondria in healthy cells, whereas green fluorescence indicates JC-1 monomers in the cytoplasm and loss of Δψm. Scale bars =100 μm.
Abbreviations: DCFH-DA, dichloro-dihydro-fluorescein diacetate; LCs, Leydig cells; NPs, nanoparticles; ROS, reactive oxygen species; SCs, Sertoli cells; h, hours.

of mitochondrial membrane potential (ΔΨm), critical for maintaining the physiological function of the respiratory chain, is usually accompanied by the production of ROS contributing to cell death. JC-1 is a cationic, lipophilic fluorescent dye used extensively to study the loss of Ψm that occurs during apoptosis.[47–49] Healthy cells showing cytoplasmic JC-1 green and mitochondrial red fluorescence are easily distinguished from apoptotic cells showing primarily cytoplasmic JC-1 green fluorescence. In our study, we observed that after exposure for 6–12 hours to ZnO NPs (15 μg/mL), a large number of LCs and SCs passed from cytoplasmic green and mitochondrial red fluorescence to cytoplasmic JC-1 green fluorescence, indicating massive loss of Δψm (Figure 6B).

ZnO NPs induce nuclear DNA leakage and breakage

Condensed and fragmented nuclei are characteristic of apoptotic cells. We utilized fluorescence microscopy to examine the nuclear dynamics of the ZnO NP-treated LCs and SCs. As shown in Figure 7, treatment of cells with ZnO NPs consistently induced nuclear DNA leakage, identified as DAPI-positive particles outside the nucleus (Figure 7A). DNA leakage became apparent at 12 hours after treatment with 15 μg/mL ZnO NPs, resulting in chromosome breaks or loss (Figure 7B, C). Approximately 27.4% and 73.9%

of LCs showed DNA leakage 24 hours after treatment with 15 and 20 μg/mL ZnO NPs, respectively (Figure 7B). Approximately 41.5% and 93.7% of SCs showed DNA leakage 24 hours after treatment with 15 and 20 μg/mL ZnO NPs, respectively (Figure 7C).

Moreover, we observed the formation of extensive γ-H2AX foci (Figure 8A, B), indicative of DNA breaks.[40,41] The occurrence of DNA damage in such cells was confirmed by the nuclear positivity for RAD51 staining (Figure 8C, D), a protein involved in the repair of DNA double-strand breaks.[42]

Western blot analyses confirmed the induction of γ-H2AX expression in LCs exposed to the higher ZnO NP concentration, but not in SCs. No detectable increase in the expression of RAD51 was observed in either cell type (Figure 8E, F). In line with our results, several studies have shown that ZnO NPs or other types of NPs induce DNA damage in a variety of cell types.[50–60]

In vivo exposure to ZnO NPs alters the structure of seminiferous tubules and spermatozoa morphologies

Various morphological and functional disorders of testes have been reported following exposure to NPs, including increased tissue oxidative stress, changes in testicular enzyme activities, and suppression of spermatogenesis.[61,62] In
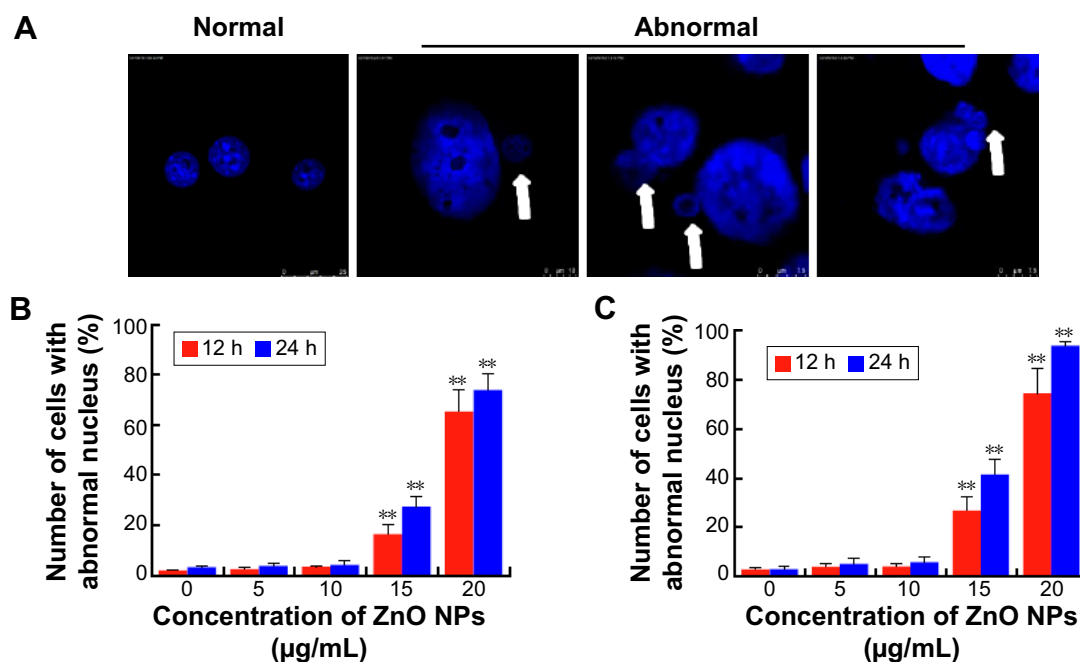
Figure 7 Nuclear DNA leakage in LCs and SCs after ZnO NP treatment.
Notes: (**A**) DAPI staining shows nuclear DNA leakage (arrows) in cells incubated in the presence of ZnO NPs. Number of LCs (**B**) and SCs (**C**) with nuclear DNA leakage after 12 and 24 hours in the presence of ZnO NPs. The results are expressed as the mean ± standard deviation of three separate experiments, in triplicate. *******P*<0.01.
Abbreviations: DAPI, 4′,6-diamidino-2-phenylindole; LCs, Leydig cells; NPs, nanoparticles; SCs, Sertoli cells; h, hours.
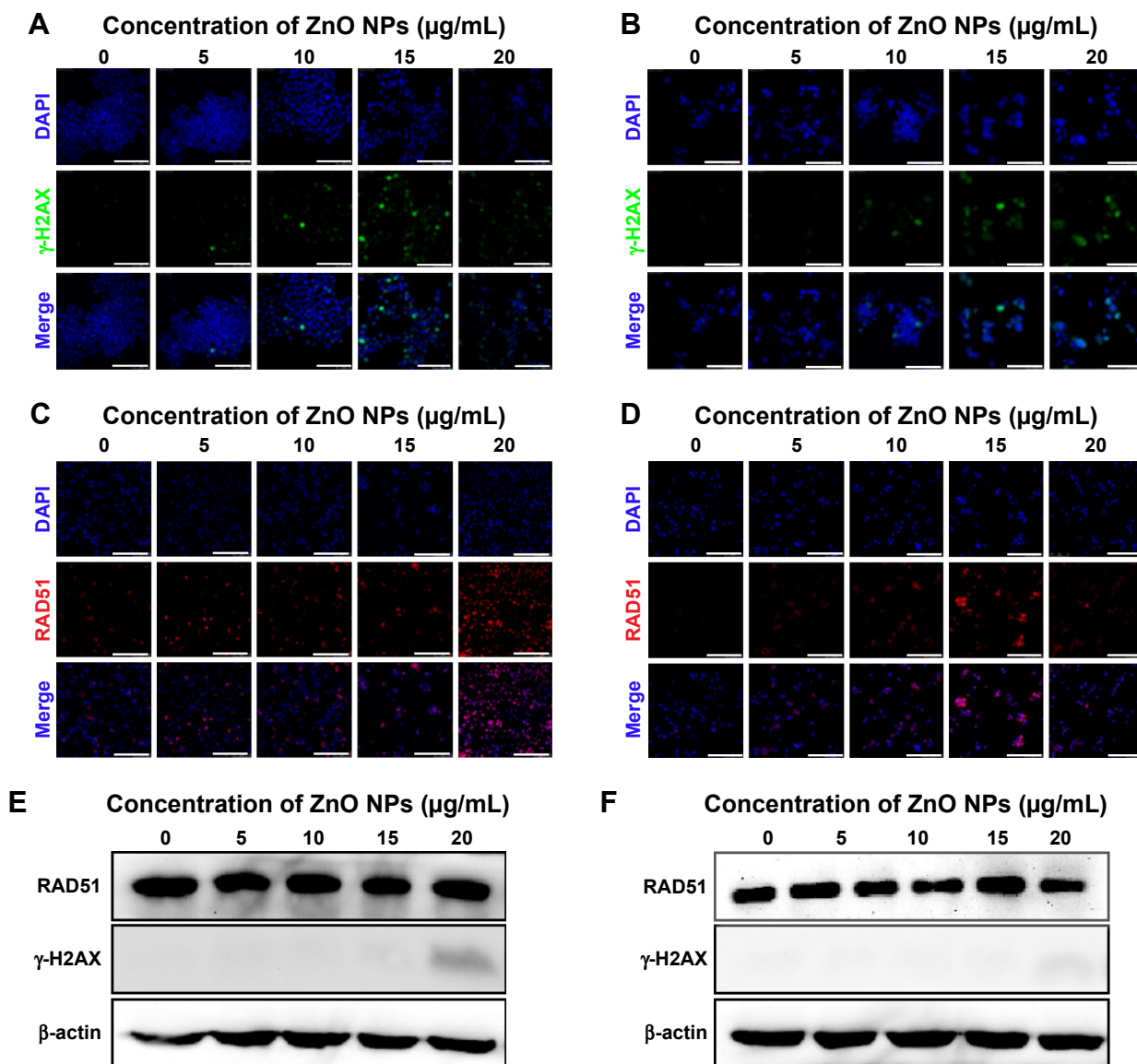
Figure 8 Nuclear DNA damage in LCs and SCs after ZnO NP treatment.
**Notes:** (**A** and **B**) Nuclear γ-H2AX foci in cells exposed in vitro to ZnO NPs for 12 hours. (**C** and **D**) Nuclear RAD51 foci in cells exposed in vitro to ZnO NPs for 12 hours. (**E** and **F**) Western blots for γ-H2AX and RAD51 in LCs and SCs. The results are expressed as the mean ± standard deviation of three separate experiments, in triplicate. (**A**, **C**, and **E**) are the data of LCs; (**B**, **D**, and **F**) are the data of SCs. Scale bars =150 μm.
Abbreviations: DAPI, 4′,6-diamidino-2-phenylindole; LCs, Leydig cells; NPs, nanoparticles; SCs, Sertoli cells.

particular, two previous studies[26,27] using exposure protocols based on daily administration of the NPs for 35 days have established that ZnO NPs have cytotoxic actions on testicular germ cells in a dose-dependent manner. In line with these studies, we found that a single systemic injection of ZnO NPs caused alteration in the structure of seminiferous epithelium and the production of morphologically abnormal spermatozoa. In fact, as shown in Figure 9A, a significant reduction in the thickness of the seminiferous epithelium was observed after injection of males with 5 mg/kg ZnO NPs at PND28 and PND42 (Figure 9B). The diameter of the seminiferous tubules was also reduced in the ZnO NP-treated

mice, although changes were slight in the group treated with 1 mg/kg ZnO NPs (Figure 9C). Moreover, the percentage of spermatozoa showing an altered morphology (double head, small head, unshaped head, double tail) at 49 days after ZnO NP treatment was significantly higher in comparison to controls ($P<0.05$ or $P<0.01$) (Figure 9D). The pictures of sperm cells that show morphological aberrations are presented in Figure S3.

The testis is typically a paired male reproductive gland that produces sperm and secretes testosterone in mammals. LCs and SCs are two important parts of the testes with critical roles in the formation of sperm. Exposure to environmental
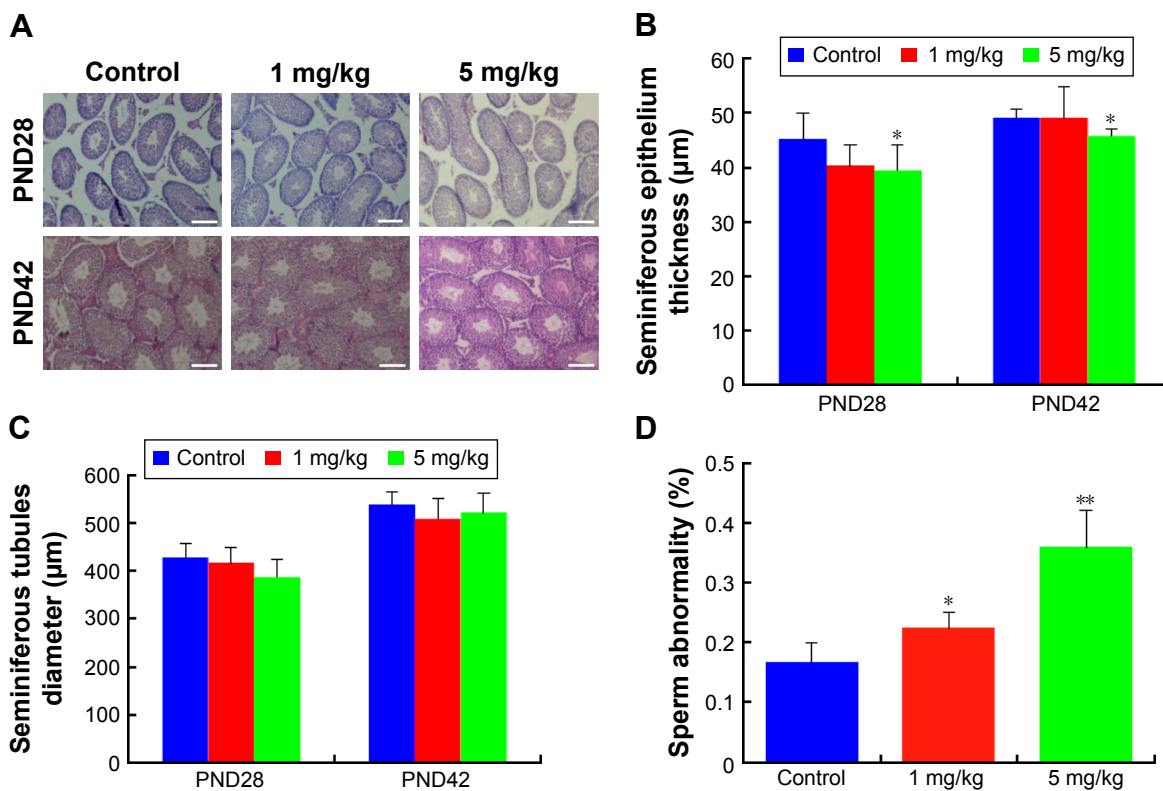
Figure 9 Structural alteration of seminiferous tubules and abnormal sperm morphologies of mice injected with ZnO NPs.
Notes: (**A**) Representative histological sections of control and treated testes. Scale bars =100 μm. (**B**) Measures of the seminiferous epithelium thickness of testicular tubules of control and treated mice. (**C**) Measures of the diameter of the seminiferous tubules of control and treated mice. (**D**) Percentage of abnormal sperm morphologies (double head, small head, unshaped head, double tail) in control and treated mice. The results are expressed as the mean ± standard deviation of three separate experiments, in triplicate. *$P<0.05$, **$P<0.01$.
Abbreviations: NPs, nanoparticles; PND, postnatal day.

toxins can affect the functions of LCs and SCs and the normal morphology, structure, and functions of the testis. Research has shown that environmental estrogens, heavy metals, phytotoxins, mycotoxins, and NPs adversely affect the testes.[63–66] Heavy metals are also common environmental toxicants that adversely affect steroid biosynthesis, causing irreversible degeneration or atrophy of the seminiferous tubules, testicular injury, and sex hormone disturbances.[26,27,67] Since the development and use of engineered NPs, many studies have examined their adverse effects on the mouse testes. Serious concerns have been expressed about the potential risks of engineered NPs, and various functional and pathological disorders and reduced sperm counts have been observed, together with the suppression of spermatogenesis, marked changes in testicular enzymes, and oxidative stress in the testes.[68,69] ZnO NPs are increasingly and widely used as a nanomaterial in many diverse disciplines. Studies have shown that ZnO NPs can change the stereological and morphometric parameters of the seminiferous tubules, reduce the number of LCs, significantly reduce the diameters of the seminiferous tubules and the height of the seminiferous

epithelium, cause maturation arrest, and increase germ cell apoptosis in the testis.[28,70]

Conclusion

These results demonstrate that ZnO NPs have the potential to induce apoptosis in testicular cells likely through DNA damage caused by ROS with possible adverse consequences for spermatogenesis and male fertility. This suggests that widespread application of ZnO NPs should be carefully assessed and precautionary measures planned out to prevent human exposures to such NPs.

Acknowledgments

Disclosure

The authors report no conflicts of interest in this work.

References

1. Zhang H, Zheng D, Ding J, Xu H, Li X, Sun W. Efficient delivery of ursolic acid by poly (N-vinylpyrrolidone)-block-poly (ε-caprolactone) nanoparticles for inhibiting the growth of hepatocellular carcinoma in vitro and in vivo. *Int J Nanomedicine*. 2015;10:1909–1920.

2. Ojha VK, Jackowski K, Abraham A, Snášel V. Dimensionality reduction, and function approximation of poly(lactic-*co*-glycolic acid) micro- and nanoparticle dissolution rate. *Int J Nanomedicine*. 2015;10:1119–1129.

3. Liu S, Zhao N, Cheng Z, Liu H. Amino-functionalized green fluorescent carbon dots as surface energy transfer biosensors for hyaluronidase. *Nanoscale*. 2015;7(15):6836–6842.

4. Aravinthan A, Govarthanan M, Selvam K, et al. Sunroot mediated synthesis and characterization of silver nanoparticles and evaluation of its antibacterial and rat splenocyte cytotoxic effects. *Int J Nanomedicine*. 2015;10:1977–1983.

5. Pelgrift RY, Friedman AJ. Nanotechnology as a therapeutic tool to combat microbial resistance. *Adv Drug Deliv Rev*. 2013;65(13–14):1803–1815.

6. Kruefu V, Wisitsoraat A, Tuantranont A, Phanichphant S. Gas sensing properties of conducting polymer/Au-loaded ZnO nanoparticle composite materials at room temperature. *Nanoscale Res Lett*. 2014;9(1):467.

7. Kim M, Lee HJ, Oh S, et al. Robust ZnO nanoparticle embedded memory device using vancomycin conjugate and its biorecognition for electrical charging node. *Biosens Bioelectron*. 2014;56:33–38.

8. Sasidharan A, Chandran P, Menon D, Raman S, Nair S, Koyakutty M. Rapid dissolution of ZnO nanocrystals in acidic cancer microenvironment leading to preferential apoptosis. *Nanoscale*. 2011;3(9):3657–3669.

9. Namvar F, Rahman HS, Mohamad R, et al. Cytotoxic effects of biosynthesized zinc oxide nanoparticles on murine cell lines. *Evid Based Complement Alternat Med*. 2015;2015:593014.

10. Saptarshi SR, Feltis BN, Wright PF, Lopata AL. Investigating the immunomodulatory nature of zinc oxide nanoparticles at sub-cytotoxic levels in vitro and after intranasal instillation in vivo. *J Nanobiotechnology*. 2015;13:6.

11. Johnson BM, Fraietta JA, Gracias DT, et al. Acute exposure to ZnO nanoparticles induces autophagic immune cell death. *Nanotoxicology*. 2015;79(6):737–748.

12. Sharma V, Shukla RK, Saxena N, Parmar D, Das M, Dhawan A. DNA damaging potential of zinc oxide nanoparticles in human epidermal cells. *Toxicol Lett*. 2009;185(3):211–218.

13. Sharma V, Singh SK, Anderson D, Tobin DJ, Dhawan A. Zinc oxide nanoparticle induced genotoxicity in primary human epidermal keratinocytes. *J Nanosci Nanotechnol*. 2011;11(5):3782–3788.

14. Lai X, Wei Y, Zhao H, et al. The effect of Fe2 O3 and ZnO nanoparticles on cytotoxicity and glucose metabolism in lung epithelial cells. *J Appl Toxicol*. 2015;35(6):651–664.

15. Lin W, Xu Y, Huang CC, Shannon KB, Chen DR, Huang YW. Toxicity of nano- and micro-sized ZnO particles in human lung epithelial cells. *J Nanopart Res*. 2009;11(1):25–39.

16. Ahamed M, Akhtar MJ, Raja M, et al. ZnO nanorod-induced apoptosis in human alveolar adenocarcinoma cells via p53, surviving and bax/bcl-2pathways: role of oxidative stress. *Nanomedicine*. 2011;7(6):904–913.

17. Ng KW, Khoo SP, Heng BC, et al. The role of the tumor suppressor p53 pathway in the cellular DNA damage response to zinc oxide nanoparticles. *Biomaterials*. 2011;32(32):8218–8225.

18. Gonzalez CR, Dorfman VB, Vitullo AD. IGF1 regulation of BOULE and CDC25A transcripts via a testosterone-independent pathway in spermatogenesis of adult mice. *Reprod Biol*. 2015;15(1):48–55.

19. Wdowiak A, Raczkiewicz D, Stasiak M, Bojar I. Levels of FSH, LH and testosterone, and sperm DNA fragmentation. *Neuro Endocrinol Lett*. 2014;35(1):73–79.

20. Payne AH, Hales DB. Overview of steroidogenic enzymes in the pathway from cholesterol to active steroid hormones. *Endocr Rev*. 2004;25(6):947–970.

21. Guttenbach M, Steinlein C, Engel W, Schmid M. Cytogenetic characterization of the SCs mouse Sertoli cell line. I. Conventional banding techniques, FISH and SKY. *Cytogenet Cell Genet*. 2001;94(1–2):71–78.

22. Sharpe RM, McKinnell C, Kivlin C, Fisher JS. Proliferation and functional maturation of Sertoli cells, and their relevance to disorders of testis function in adulthood. *Reproduction*. 2003;125(6):769–784.

23. Nakamura D, Yanagiba Y, Duan Z, et al. Bisphenol A may cause testosterone reduction by adversely affecting both testis and pituitary systems similar to estradiol. *Toxicol Lett*. 2010;194(1–2):16–25.

24. Savchuk I, Söder O, Svechnikov K. Mono-2-ethylhexyl phthalate stimulates androgen production but suppresses mitochondrial function in mouse Leydig cells with different steroidogenic potential. *Toxicol Sci*. 2015;145(1):149–156.

25. Sekaran S, Jagadeesan A. In utero exposure to phthalate downregulates critical genes in Leydig cells of F1 male progeny. *J Cell Biochem*. 2015;116(7):1466–1477.

26. Ji X, Li Z, Chen H, et al. Cytotoxic mechanism related to dihydrolipoamide dehydrogenase in Leydig cells exposed to heavy metals. *Toxicology*. 2015;334:22–32.

27. Marettová E, Maretta M, Legáth J. Toxic effects of cadmium on testis of birds and mammals: a review. *Anim Reprod Sci*. 2015;155:1–10.

28. Talebi AR, Khorsandi L, Moridian M. The effect of zinc oxide nanoparticles on mouse spermatogenesis. *J Assist Reprod Genet*. 2013;30(9):1203–1209.

29. Zhang XF, Choi YJ, Han JW, et al. Differential nanoreprotoxicity of silver nanoparticles in male somatic cells and spermatogonial stem cells. *Int J Nanomedicine*. 2015;10:1335–1357.

30. Carré-Rangel L, Alonso-Nuñez G, Espinoza-Gómez H, Flores-López LZ. Green synthesis of silver nanoparticles: effect of dextran molecular weight used as stabilizing-reducing agent. *J Nanosci Nanotechnol*. 2015;15(12):9849–9855.

31. Wojnarowicz J, Kusnieruk S, Chudoba T, et al. Paramagnetism of cobalt-doped ZnO nanoparticles obtained by microwave solvothermal synthesis. *Beilstein J Nanotechnol*. 2015;6:1957–1969.

32. Selvarajan E, Mohanasrinivasan V. Biosynthesis and characterization of ZnO nanoparticles using Lactobacillus plantarum VITES07. *Mater Lett*. 2013;112:180–182.

33. Kumar H, Rani R. Development of biosensors for the detection of biological warfare agents: its issues and challenges. *Sci Prog*. 2013;96(Pt 3):294–308.

34. Jayaseelan C1, Rahuman AA, Kirthi AV, et al. Novel microbial route to synthesize ZnO nanoparticles using *Aeromonas hydrophila* and their activity against pathogenic bacteria and fungi. *Spectrochem Acta A Mol Biomol Spect*. 2012;90:78–84.

35. Eita M, El Sayed R, Muhammed M. Optical properties of thin films of zinc oxide quantum dots and polydimethylsiloxane: UV-blocking and the effect of cross-linking. *J Colloid Interface Sci*. 2012;387(1):135–140.

36. Yu KN, Yoon TJ, Minai-Tehrani A, et al. Zinc oxide nanoparticle induced autophagic cell death and mitochondrial damage via reactive oxygen species generation. *Toxicol In Vitro*. 2013;27(4):1187–1195.

37. Colvin VL. The potential environmental impact of engineered nanomaterials. *Nat Biotechnol*. 2013;21(10):1166–1170.

38. Yang P, Chen H, Tsai J, Lin L. Cadmium induces Ca2+-dependent necrotic cell death through calpain-triggered mitochondrial depolarization and reactive oxygen species-mediated inhibition of nuclear factor-κB activity. *Chem Res Toxicol*. 2007;20(3):406–415.

39. Circu ML, Aw TY. Reactive oxygen species, cellular redox systems, and apoptosis. *Free Radic Biol Med*. 2010;48(6):749–762.

40. Nguyen KC, Willmore WG, Tayabali AF. Cadmium telluride quantum dots cause oxidative stress leading to extrinsic and intrinsic apoptosis in hepatocellular carcinoma HepG2 cells. *Toxicology*. 2013;306:114–123.

41. Simon HU, Haj-Yehia A, Levi-Schaffer F. Role of reactive oxygen species (ROS) in apoptosis induction. *Apoptosis*. 2000;5(5):415–418.

42. De Berardis B, Civitelli G, Condello M, et al. Exposure to ZnO nanoparticles induces oxidative stress and cytotoxicity in human colon carcinoma cells. *Toxicol Appl Pharmacol*. 2010;246(3):116–127.

43. Chen HT, Bhandoola A, Difilippantonio MJ, et al. Response to RAG-mediated VDJ cleavage by NBS1 and γH2AX. *Science*. 2000; 290(5498):1962–1965.

44. Baldock RA, Day M, Wilkinson OJ, et al. ATM localization and heterochromatin repair depend on direct interaction of the 53BP1-BRCT2 domain with γH2AX. *Cell Rep*. 2015;13(10):2081–2089.

45. Wahab R, Siddiqui MA, Saquib Q, et al. ZnO nanoparticles induced oxidative stress and apoptosis in HepG2 and MCF-7 cancer cells and their antibacterial activity. *Colloids Surf B Biointerfaces*. 2014;117: 267–276.

46. Sharma V, Anderson D, Dhawan A. Zinc oxide nanoparticles induce oxidative DNA damage and ROS-triggered mitochondria mediated apoptosis in human liver cells (HepG2). *Apoptosis*. 2012;17(8):852–870.

47. Ishikawa K, Takenaga K, Akimoto M, et al. ROS-generating mitochondrial DNA mutations can regulate tumor cell metastasis. *Science*. 2008;320(5876):661–664.

48. Zorov DB, Filburn CR, Klotz LO, Zweier JL, Sollott SJ. Reactive oxygen species (ROS)-induced ROS release: a new phenomenon accompanying induction of the mitochondrial permeability transition in cardiac myocytes. *J Exp Med*. 2000;192(7):1001–1014.

49. Turrens JF. Mitochondrial formation of reactive oxygen species. *J Physiol*. 2003;552(Pt 2):335–344.

50. Chiang HM, Xia Q, Zou X, et al. Nanoscale ZnO induces cytotoxicity and DNA damage in human cell lines and rat primary neuronal cells. *J Nanosci Nanotechnol*. 2012;12(3):2126–2135.

51. Wang CC, Wang S, Xia Q, et al. Phototoxicity of zinc oxide nanoparticles in HaCaT keratinocytes-generation of oxidative DNA damage during UVA and visible light irradiation. *J Nanosci Nanotechnol*. 2013; 13(6):3880–3888.

52. Demir E, Creus A, Marcos R. Genotoxicity and DNA repair processes of zinc oxide nanoparticles. *J Toxicol Environ Health A*. 2014;77(21): 1292–1303.

53. Uzar NK, Abudayyak M, Akcay N, Algun G, Özhan G. Zinc oxide nanoparticles induced cyto- and genotoxicity in kidney epithelial cells. *Toxicol Mech Methods*. 2015;25(4):334–339.

54. Zijno A, De Angelis I, De Berardis B, et al. Different mechanisms are involved in oxidative DNA damage and genotoxicity induction by ZnO and TiO2 nanoparticles in human colon carcinoma cells. *Toxicol In Vitro*. 2015;29(7):1503–1512.

55. Govindaraju K, Krishnamoorthy K, Alsagaby SA, Singaravelu G, Premanathan M. Green synthesis of silver nanoparticles for selective toxicity towards cancer cells. *IET Nanobiotechnol*. 2015;9(6): 325–330.

56. Sambandam B, Devasena T, Islam VI, Prakhya BM. Characterization of coal fly ash nanoparticles and their induced in vitro cellular toxicity and oxidative DNA damage in different cell lines. *Indian J Exp Biol*. 2015; 53(9):585–593.

57. Lua CF, Yuana XY, Lia LZ, et al. Combined exposure to nano-silica and lead induced potentiation of oxidative stress and DNA damage in human lung epithelial cells. *Ecotoxicol Environ Saf*. 2015;122:537–544.

58. Yao X, Huang C, Chen X, Yi Z, Sanche L. Chemical radiosensitivity of DNA induced by gold nanoparticles. *J Biomed Nanotechnol*. 2015; 11(3):478–485.

59. Tabei Y, Sonoda A, Nakajima Y, et al. Intracellular accumulation of indium ions released from nanoparticles induces oxidative stress, proinflammatory response and DNA damage. *J Biochem*. 2016;159(2): 225–237.

60. Carmona ER, Inostroza-Blancheteau C, Rubio L, Marcos R. Genotoxic and oxidative stress potential of nanosized and bulk zinc oxide particles in Drosophila melanogaster. *Toxicol Ind Health*. Epub 2015 Sep 29.

61. Zhang LD, Li HC, Chong T, et al. Prepubertal exposure to genistein alleviates di-(2-ethylhexyl) phthalate induced testicular oxidative stress in adult rats. *Biomed Res Int*. 2014;2014:598630.

62. Wisniewski P, Romano RM, Kizys MM, et al. Adult exposure to bisphenol A (BPA) in Wistar rats reduces sperm quality with disruption of the hypothalamic-pituitary-testicular axis. *Toxicology*. 2015; 329:1–9.

63. Li X, Li H, Jia L, Li X, Rahman N. Oestrogen action and male fertility: experimental and clinical findings. *Cell Mol Life Sci*. 2015;72(20): 3915–3930.

64. Manfo FP, Nantia EA, Mathur PP. Effect of environmental contaminants on mammalian testis. *Jia Curr Mol Pharmacol*. 2014;7(2):119–135.

65. Lan Z, Yang WX. Jia Nanoparticles and spermatogenesis: how do nanoparticles affect spermatogenesis and penetrate the blood-testis barrier. *Nanomedicine (Lond)*. 2012;7(4):579–596.

66. Wang Y, Zheng W, Bian X, et al. Zearalenone induces apoptosis and cytoprotective autophagy in primary Leydig cells. *Toxicol Lett*. 2014;226(2):182–191.

67. Rana SV. Perspectives in endocrine toxicity of heavy metals. *Biol Trace Elem Res*. 2014;160(1):1–14.

68. Meena R, Kajal K, Paulraj R. Cytotoxic and genotoxic effects of titanium dioxide nanoparticles in testicular cells of male Wistar rat. *Appl Biochem Biotechnol*. 2015;175(2):825–840.

69. Hong F, Si W, Zhao X, et al. TiO₂ nanoparticle exposure decreases spermatogenesis via biochemical dysfunctions in the testis of male mice. *J Agric Food Chem*. 2015;63(31):7084–7092.

70. Moridian M, Khorsandi L, Talebi AR. Morphometric and stereological assessment of the effects of zinc oxide nanoparticles on the mouse testicular tissue. *Bratisl Lek Listy*. 2015;116(5):321–325.

Supplementary materials

A

Concentration of ZnO NPs (µg/mL)
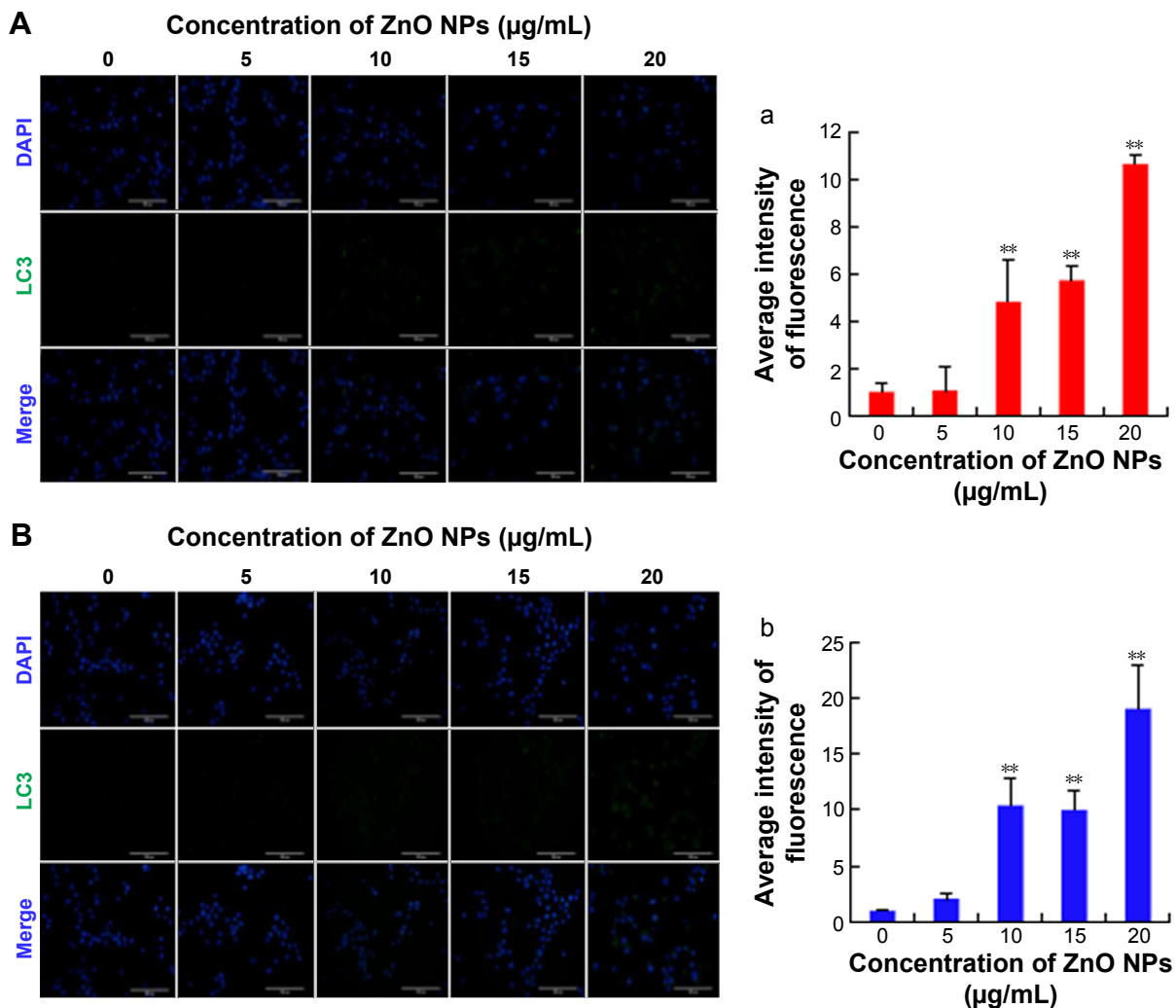
Figure S1 ZnO NPs exposure increases autophagy in cultured LC and SC cell lines in 12 h.
Notes: (**A**) LC3-stained LCs: (a) the average intensity of LC3 fluorescence in LCs. (**B**) LC3-stained SCs: (b) the average intensity of LC3 fluorescence in SCs. Scale bars =100 µm. **$P<0.01$.
**Abbreviations:** DAPI, 4′,6-diamidino-2-phenylindole; LCs, Leydig cells; NPs, nanoparticles; SCs, Sertoli cells.
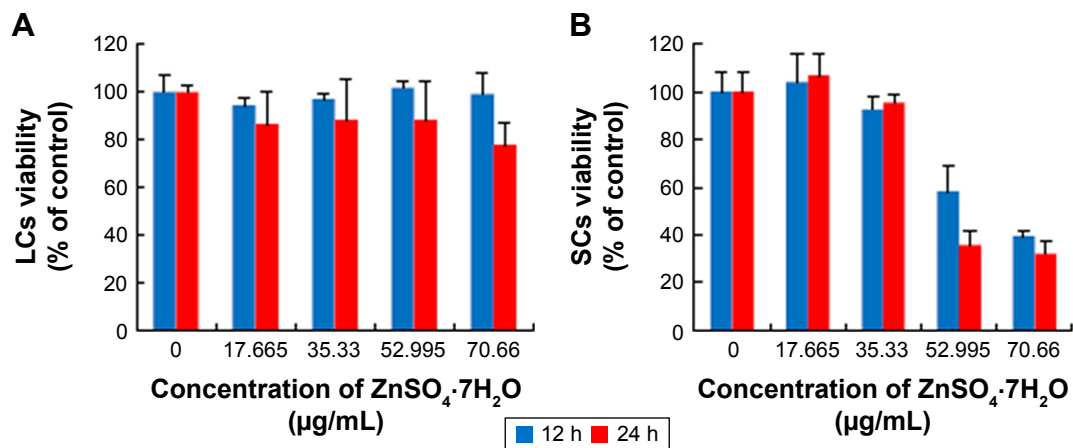
Figure S2 (*Continued*)

C

D
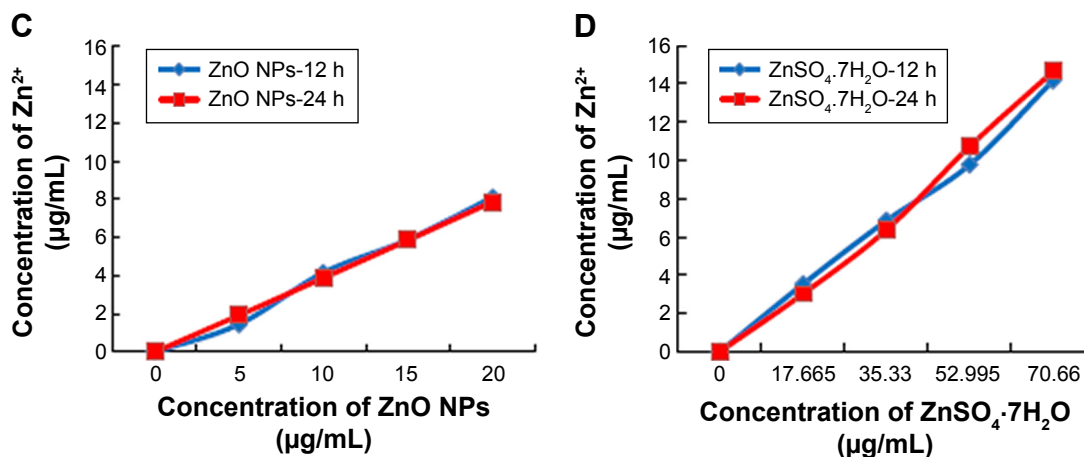
Figure S2 Toxicity of ZnSO$_4$·7H$_2$O for LCs and SCs, and dissolution curve of Zn^{2+} from different concentrations of ZnO NPs and ZnSO$_4$·7H$_2$O in medium.
Notes: (**A** and **B**) In order to verify ZnSO$_4$·7H$_2$O cytotoxicity, cells were treated with various concentrations of ZnSO$_4$·7H$_2$O for 12 and 24 hours, and viability determined with MTT. MTT indicated time- and concentration-dependent cytotoxicity of ZnSO$_4$·7H$_2$O on both cell lines. On comparing the effects of ZnO NPs on the two cell lines with the MTT assay, the ZnO NPs showed hazardous effects than ZnSO$_4$·7H$_2$O. (**C**) Dissolution curve of Zn^{2+} from different concentrations of ZnO NPs in medium. (**D**) Dissolution curve of Zn^{2+} from different concentrations of ZnSO$_4$·7H$_2$O in medium. More Zn^{2+} was released from ZnSO$_4$·7H$_2$O than ZnO NPs at the highest concentration. This shows that the ZnO NP toxicity was dependent on the particle and not on the released Zn^{2+}. Also, 17.665, 35.33, 52.995, and 70.66 µg/mL ZnSO$_4$·7H$_2$O have the same concentration zinc with 5, 10, 15, and 20 µg/mL ZnO NPs, respectively. The results are expressed as the mean ± standard deviation of three separate experiments.
Abbreviations: LCs, Leydig cells; MTT, 3-(4,5-dimethylthiazol-2-yl)-2,5-diphenyltetrazolium bromide; NPs, nanoparticles; SCs, Sertoli cells; h, hours.
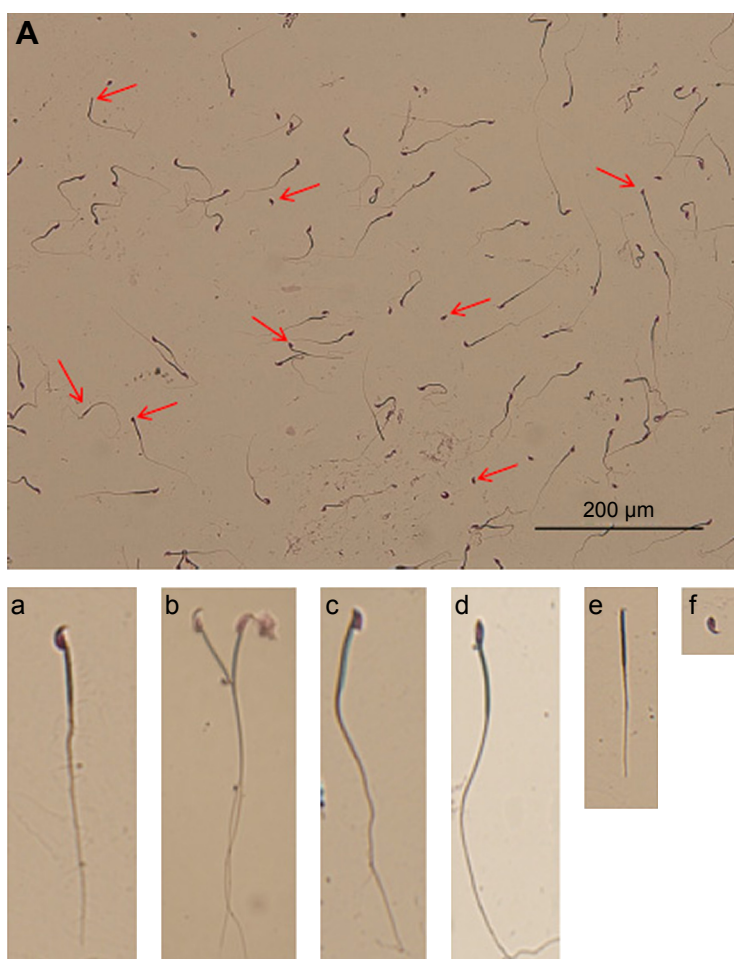
Figure S3 Picture of sperm morphologies.
Notes: (**A**) Picture of sperm morphologies and abnormal sperm (red arrows). (a) Normal sperm. (b) Abnormal sperm with two heads and two tails. (c, d) Abnormal sperm with head deformities. (e) Abnormal sperm with no head. (f) Abnormal sperm with no tail.